Diagnostic Potential of Supplemental Static and Dynamic ^{68}Ga-FAPI-46 PET for Primary ^{18}F-FDG–Negative Pulmonary Lesions

Manuel Röhrich[1–3], Johanna Daum[1,3], Ewgenija Gutjahr[4], Anna-Maria Spektor[1,3], Frederik M. Glatting[1,5,6], Yasemin Aylin Sahin[2], Hans Georg Buchholz[2], Jorge Hoppner[1,3], Cathrin Schroeter[1,3], Eleni Mavriopoulou[1,3], Kai Schlamp[3,7], Matthias Grott[3,8], Florian Eichhorn[3,8], Claus Peter Heußel[3,7], Hans Ulrich Kauczor[3,9,10], Michael Kreuter[11,12], Frederik Giesel[1,3,13–15], Mathias Schreckenberger[2], Hauke Winter[3,7] and Uwe Haberkorn[1,3,9,16]

[1]Department of Nuclear Medicine, University Hospital Heidelberg, Heidelberg, Germany; [2]Department of Nuclear Medicine, University Hospital Mainz, Mainz, Germany; [3]German Center of Lung Research, Heidelberg, Germany; [4]Institute of Pathology, University Hospital Heidelberg, Heidelberg, Germany; [5]Clinical Cooperation Unit Molecular and Radiation Oncology, German Cancer Research Center, Heidelberg, Germany; [6]Department of Radiation Oncology, University Hospital Heidelberg, Heidelberg, Germany; [7]Department of Radiology, Thoraxklinik, University Hospital Heidelberg, Heidelberg, Germany; [8]Department of Thoracic Surgery, Thoraxklinik, University Hospital Heidelberg, Heidelberg, Germany; [9]Department of Diagnostic and Interventional Radiology, University Hospital Heidelberg, Heidelberg, Germany; [10]Center for Interstitial and Rare Lung Diseases, Pneumology, and Respiratory Critical Care Medicine, Thoraxklinik, University of Heidelberg, Heidelberg, Germany; [11]Department of Pneumology, Mainz Center for Pulmonary Medicine, Mainz University, Mainz, Germany; [12]Medical Center and Department of Pulmonary, Critical Care, and Sleep Medicine, Marienhaus Clinic Mainz, Mainz, Germany; [13]Department of Nuclear Medicine, Medical Faculty, University Hospital Düsseldorf, Heinrich Heine University, Düsseldorf, Germany; [14]Institute for Radiation Sciences, Osaka University, Osaka, Japan; [15]German Cancer Consortium, Heidelberg, Germany; and [16]Clinical Cooperation Unit Nuclear Medicine, German Cancer Research Center, Heidelberg, Germany

PET using ^{68}Ga-labeled fibroblast activation protein (FAP) inhibitors (FAPIs) holds high potential for diagnostic imaging of various malignancies, including lung cancer (LC). However, ^{18}F-FDG PET is still the clinical gold standard for LC imaging. Several subtypes of LC, especially lepidic LC, are frequently ^{18}F-FDG PET–negative, which markedly hampers the assessment of single pulmonary lesions suggestive of LC. Here, we evaluated the diagnostic potential of static and dynamic ^{68}Ga-FAPI-46 PET in the ^{18}F-FDG–negative pulmonary lesions of 19 patients who underwent surgery or biopsy for histologic diagnosis after PET imaging. For target validation, FAP expression in lepidic LC was confirmed by FAP immunohistochemistry. **Methods:** Hematoxylin and eosin staining and FAP immunohistochemistry of 24 tissue sections of lepidic LC from the local tissue bank were performed and analyzed visually. Clinically, 19 patients underwent static and dynamic ^{68}Ga-FAPI-46 PET in addition to ^{18}F-FDG PET based on individual clinical indications. Static PET data of both examinations were analyzed by determining SUV_{max}, SUV_{mean}, and tumor-to-background ratio (TBR) against the blood pool, as well as relative parameters (^{68}Ga-FAPI-46 in relation to ^{18}F-FDG), of histologically confirmed LC and benign lesions. Time–activity curves and dynamic parameters (time to peak, slope, k_1, k_2, k_3, and k_4) were extracted from dynamic ^{68}Ga-FAPI-46 PET data. The sensitivity and specificity of all parameters were analyzed by calculating receiver-operating-characteristic curves. **Results:** FAP immunohistochemistry confirmed the presence of strongly FAP-positive cancer-associated fibroblasts in lepidic LC. LC showed markedly elevated ^{68}Ga-FAPI-46 uptake, higher TBRs, and higher ^{68}Ga-FAPI-46–to–^{18}F-FDG ratios for all parameters than did benign pulmonary lesions. Dynamic imaging analysis revealed differential time–activity curves for LC and benign pulmonary lesions: initially increasing time–activity curves with a decent slope were typical of LC, and steadily decreasing time–activity curve indicated benign pulmonary lesions, as was reflected by a significantly increased time to peak and significantly smaller absolute values of the slope for LC. Relative ^{68}Ga-FAPI-46–to–^{18}F-FDG ratios regarding SUV_{max} and TBR showed the highest sensitivity and specificity for the discrimination of LC from benign pulmonary lesions. **Conclusion:** ^{68}Ga-FAPI-46 PET is a powerful new tool for the assessment of single ^{18}F-FDG–negative pulmonary lesions and may optimize patient stratification in this clinical setting.

Key Words: fibroblast activation protein; FAPI; PET; lung cancer; pulmonary lesions

J Nucl Med 2024; 65:872–879
DOI: 10.2967/jnumed.123.267103

Lung cancer (LC) is the most frequently occurring type of cancer and is associated with a high rate of cancer-related death worldwide (*1*). Accurate and timely diagnosis of LC is crucial for treatment stratification of patients. CT is the most frequently used imaging method for primary staging of LC. CT imaging can be supplemented by ^{18}F-FDG PET to improve tumor staging or to further characterize suggestive pulmonary lesions. Although tumor staging is clearly improved by ^{18}F-FDG PET compared with CT, the additional diagnostic value of ^{18}F-FDG for characterization of suggestive pulmonary lesions is limited (*2*). Different subtypes of LC have been shown to exhibit largely variable ^{18}F-FDG avidity, such as lepidic LC, which are frequently ^{18}F-FDG–negative, or other acinar- or papillary-dominant adenocarcinomas, which are

Received Nov. 24, 2023; revision accepted Feb. 20, 2024.
For correspondence or reprints, contact Manuel Röhrich (manuel.roehrich@med.uni-heidelberg.de).
Published online Apr. 11, 2024.

^{18}F-FDG–negative or show low ^{18}F-FDG avidity in a substantial percentage of cases (*3*,*4*).

PET with ^{68}Ga- or ^{18}F-labeled fibroblast activation protein (FAP) inhibitors (FAPIs) has recently been introduced as a novel imaging technique for various cancers and nonmalignant diseases with tissue remodeling (*5*–*9*). Although the clinically well-established ^{18}F-FDG PET is based on increased glucose metabolism of neoplastic cells, FAPI PET allows visualization of the stromal tumor compartment in terms of FAP-positive fibroblasts (*9*). Because of the vast stromal portion and minor neoplastic-cell portion in many epithelial tumor entities, including LC, FAPIs have a high tumor accumulation in these types of cancer (*10*–*13*). Several studies have compared the diagnostic performance of FAPI PET and ^{18}F-FDG PET with respect to the imaging properties of both PET examinations and with respect to potential additional FAPI-positive findings that may lead to differential staging (*14*,*15*). In consideration of LC, previous studies have focused on patients with advanced LC and evaluated staging on the basis of FAPI PET compared with ^{18}F-FDG or CT imaging (*13*,*16*–*18*). To our knowledge, no evaluation of FAPI PET yet exists focusing on the characterization of single suggestive pulmonary lesions in the primary situation. Here, we applied static and dynamic ^{68}Ga-FAPI-46 PET imaging in 19 treatment-naïve patients with ^{18}F-FDG PET–negative suggestive pulmonary lesions. All patients underwent biopsy or surgical histologic confirmation of their lesions after imaging. For target validation, FAP expression patterns in 24 separate cases of lepidic LC were evaluated by FAP immunohistochemistry. The purpose of this analysis was to demonstrate the potential diagnostic benefit of supplemental ^{68}Ga-FAPI-46 PET for primary assessment of patients with single suggestive pulmonary lesions.

MATERIALS AND METHODS

Patients

Between February 2022 and April 2023, 19 patients with suggestive pulmonary lesions were examined by CT, ^{18}F-FDG PET, and ^{68}Ga-FAPI-46 PET at the University Hospital Heidelberg. All patients underwent CT and ^{18}F-FDG PET as clinical routine scans and were individually referred for additional ^{68}Ga-FAPI-46 PET by their treating physicians because of inconclusive findings on CT and ^{18}F-FDG PET (^{18}F-FDG negativity despite suggestive CT morphology or patient-related risk factors according to the Fleischner Society guidelines (*19*)). Written informed consent was obtained from all patients on an individual-patient basis following the regulations of the German Pharmaceuticals Act §13(2b). After imaging, all patients underwent resection or biopsy of their pulmonary lesions followed by histopathologic diagnosis. Retrospective analysis of imaging, clinical, and pathologic data was approved by the local institutional review board (study number S-115/2020).

Diagnostic CT, ^{18}F-FDG PET/CT, and ^{68}Ga-FAPI-46 PET

All 19 patients underwent diagnostic contrast-enhanced CT imaging of the chest before PET imaging. ^{18}F-FDG PET/CT was performed according to standard care as previously described (*14*). ^{68}Ga-FAPI-46 was synthesized and labeled according to established protocols (*9*). Static and dynamic ^{68}Ga-FAPI-46 PET/CT was performed using a Biograph mCT Flow scanner (Siemens) as previously described (*20*). In short, after injection of 187–329 MBq of ^{68}Ga-labeled FAPI-46, low-dose CT without contrast medium was performed, followed by dynamic PET (28 frames over 60 min) to characterize tracer uptake over time, followed by whole-body PET/CT 60 min after tracer injection in 16 of 19 patients. In 3 patients, only whole-body PET/CT 60 min after tracer injection was performed. Reconstructions were performed with corrections for scatter, decay, and attenuation. The average time (±SD) between ^{18}F-FDG PET/CT and ^{68}Ga-FAPI-46 PET/CT was 6.2 ± 6.4 d.

Image Analysis

For static ^{18}F-FDG PET/CT and ^{68}Ga-FAPI-46 PET/PET/CT data, all pulmonary lesions were contoured manually on the basis of their CT appearance. For all lesions, SUV_{max}, SUV_{mean}, and tumor-to-background ratio (TBR) against blood pool, as well as relative parameters (^{68}Ga-FAPI-46 in relation to ^{18}F-FDG), were calculated. All cases selected for this analysis were classified as ^{18}F-FDG–negative according to lesional ^{18}F-FDG uptake equal to or below the blood pool level (in terms of a maximum and mean TBR of less than 1.3) as previously published (*21*). Differences between histologically confirmed LC and benign lesions were analyzed. For dynamic ^{68}Ga-FAPI-46 PET data, time–activity curves and quantitative dynamic parameters (time to peak [time between start of the dynamic image acquisition and the frame with the highest activity] and slope [relative gradient between the time–activity curve peak and the lowest activity of the following time–activity curve section in analogy to

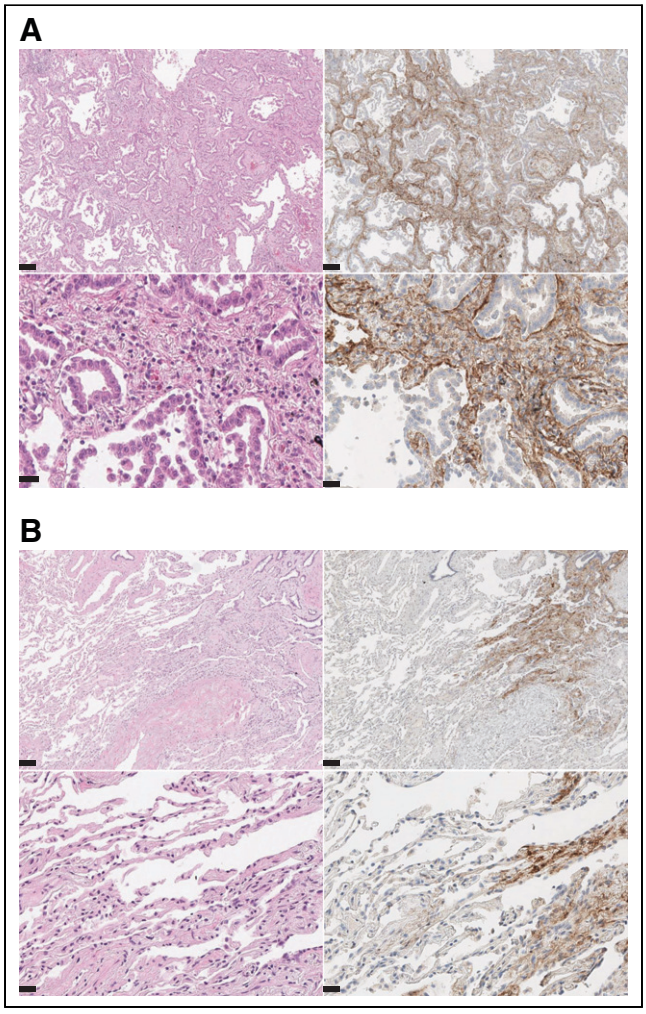

FIGURE 1. FAP expression in lepidic LC. (A and B) Representative hematoxylin and eosin staining (left) and immunohistochemical staining against FAP (right) of central part of lepidic LC biopsy, which shows strong stromal FAP positivity (A), and tumor front of lepidic LC, showing transition from FAP-positive LC tumor rim into FAP-negative physiologic lung tissue (B) (magnification: upper rows, ×10; lower rows, ×40) (scale bars: upper rows, 100 μm; lower rows, 20 μm).

TABLE 1
Clinical Parameters and Diagnoses of 19 Patients with ^{18}F-FDG–Negative Pulmonary Lesions

Patient no.	Age (y)	Sex	Dynamic PET imaging	Localization	Largest diameter (mm)	Histologic confirmation	Diagnosis	Growth pattern	TNM stage
1	64	M	No	Right upper lobe	20	Wedge resection	Tuberculosis	Not applicable	Not applicable
2	73	M	Yes	Left hilus	14	Bronchoscopy with biopsy	Calcified lymph node	Not applicable	Not applicable
3	68	F	Yes	Right lower lobe	29	Lobectomy	Adenocarcinoma	Lepidic	T1cN0M0
4	58	M	Yes	Right upper lobe	10	Wedge resection	Granuloma	Not applicable	Not applicable
5	75	M	Yes	Left lower lobe	16	Lobectomy	Adenocarcinoma	Acinar/lepidic	T1bN0M0
6	70	F	Yes	Left lower lobe	23	Lobectomy	Adenocarcinoma	Acinar	T1cN0M0
7	62	M	Yes	Right lower lobe	79	Lobectomy	Sarcoidosis	Not applicable	Not applicable
8	50	M	Yes	Left upper lobe	13	CT-guided biopsy	Adenocarcinoma	Acinar	T1bN0M0
9	57	F	Yes	Right lower lobe	17	Lobectomy	Adenocarcinoma	Acinar	T1cN0M0
10	63	M	Yes	Right upper lobe	15	CT-guided biopsy	Adenocarcinoma	Acinar	T1bN1M0
11	41	M	No	Left lower lobe	17	Wedge resection	Hamartoma	Not applicable	Not applicable
12	45	M	Yes	Right lower lobe	16	Enucleation	Hamartoma	Not applicable	Not applicable
13	70	M	Yes	Right upper lobe	16	Lobectomy	Adenocarcinoma	Acinar	T2aN0M0
14	72	M	Yes	Left upper lobe	23	Lobectomy	Adenocarcinoma	Acinar	T1bN0M0
15	65	M	Yes	Right upper lobe	29	Lobectomy	Adenocarcinoma	Lepidic	T1cN0M0
16	50	M	No	Right lower lobe	18	CT-guided biopsy	Typical carcinoid	Not applicable	T1bN0M0
17	51	F	Yes	Right upper lobe	29	CT-guided biopsy	Adenocarcinoma	Lepidic/acinar	T2aN0M0
18	64	F	Yes	Left upper lobe	28	Segment resection	Adenocarcinoma	Lepidic	T1aN0M0
19	77	M	Yes	Left lower lobe	15	CT-guided biopsy	Lung tissue	Not applicable	Not applicable

previously published dynamic PET data analyses (*22*)]) were extracted, and differences between histologically confirmed LC and benign lesions were analyzed. All image analysis was performed using PMOD software (version 4.1; PMOD Technologies).

Immunohistochemistry

To validate FAP expression in lepidic LC, 24 tissue sections of histologically proven lepidic LC from the local tissue bank were stained for hematoxylin and eosin and FAP. These 24 cases were not examined by ^{68}Ga-FAPI-46 PET/CT. For FAP immunohistochemistry, semithin tissue sections of 4-μm thickness were prepared from corresponding paraffin blocks being generated from resection tissue after its fixation in 4% buffered formalin for 24 h at room temperature. Tissue sections were treated with cell conditioning 2 (Roche) buffer (pH 8.0) for antigen retrieval. Immunohistochemical staining was performed using the antibody anti–FAP-α (1:100; Abcam [catalog no. ab207178]). Automated immunostaining was done using the automated Ventana BenchMark Ultra with the OptiView DAB Kit (Roche), Dako Autostainer-Link 48, and the EnVision Flex Kit (Agilent). Stained tissue sections were mounted with Consul-Mount (Thermo Fisher Scientific) and scanned by Aperio AT2 (Leica; magnification 1:400) for analysis. All samples were provided by the Tissue Bank of the National Center for Tumor Diseases, in accordance with the regulations of the tissue bank and the approval of the ethics committee of Heidelberg University.

Statistical Analysis

We performed descriptive analyses for patients and their characteristics. For determination of static and dynamic PET parameters, median and range were used. For determination of significance, a 2-sided *t* test was used, and *P* values of less than 0.05 were defined as statistically significant. Receiver-operating-characteristic curves and corresponding estimates of area under the curve, including 95% CIs, were computed for static and dynamic PET parameters. GraphPad Prism, version 10, was used for all statistical analyses.

RESULTS

Target Confirmation of FAP in Lepidic LC

To evaluate FAP expression in lepidic LC, we performed FAP immunohistochemistry of 24 biopsy samples of lepidic LC. In all samples, we found variably intensive FAP-positive areas. FAP positivity was particularly pronounced in stroma-rich tumor areas (Fig. 1A) but was also clearly detectable in the tumor rim within single alveolar septa, which showed a desmoplastic reaction to the tumor (Fig. 1B). In contrast, adjacent lung tissue was fully FAP-negative (Fig. 1B).

Patient Characteristics and Histologic Results

The cohort consisted of 19 patients (5 female, 14 male) aged from 41 to 77 y (average, 61.8 ± 10.5 y). The average size of the CT-graphically suggestive lesions was 22.47 ± 14.9 mm. After ^{18}F-FDG and ^{68}Ga-FAPI-46 PET imaging, tissue from all patients was obtained by either biopsy or surgery and subjected to definitive pathologic diagnosis. Seven patients had benign diagnoses

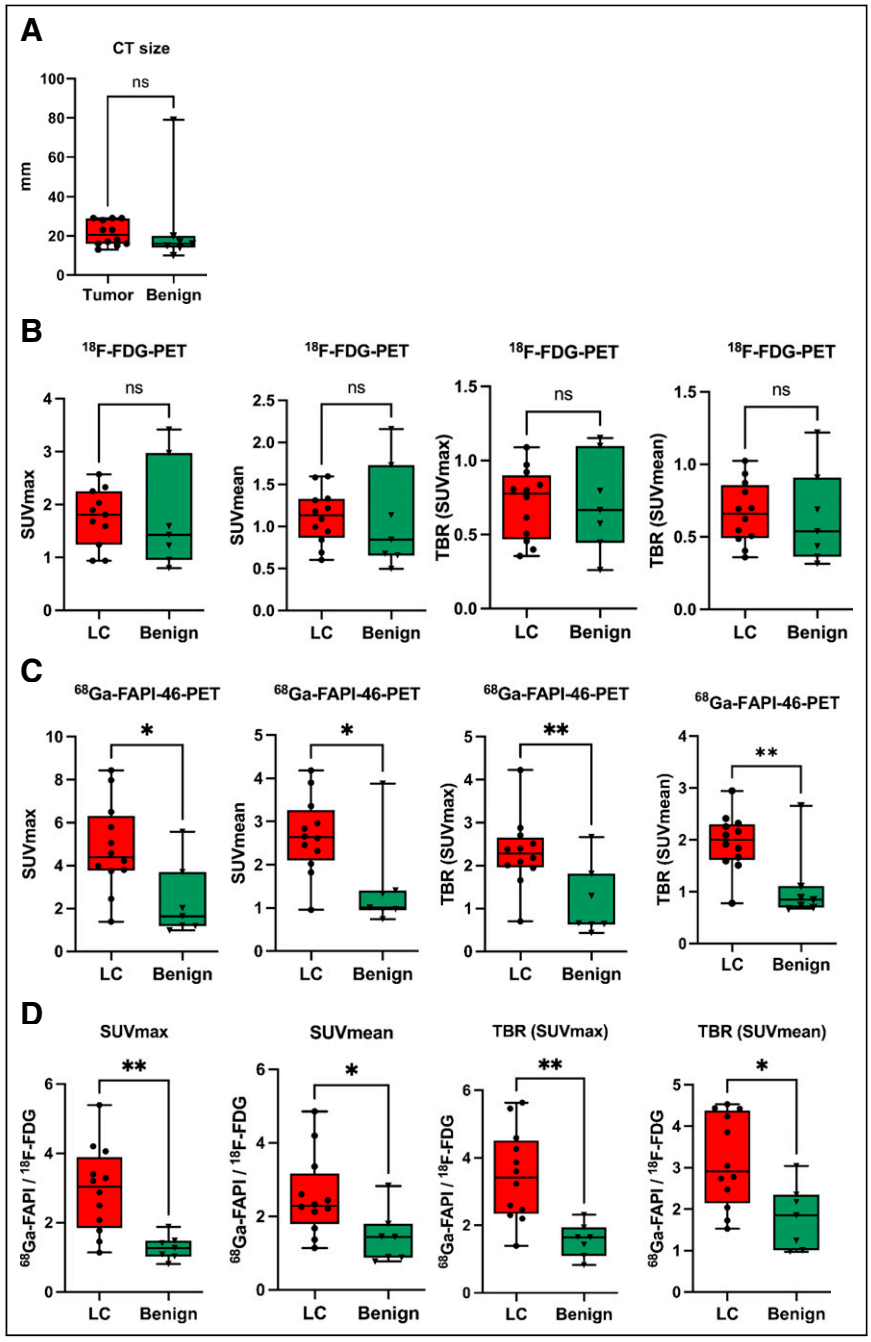

FIGURE 2. Quantitative analysis of ^{18}F-FDG and ^{68}Ga-FAPI-46 uptake in LC and benign pulmonary lesions of 19 patients. (A–C) Box plots of SUV_{max}, SUV_{mean}, and their corresponding TBRs against mediastinal blood pool for LC and benign pulmonary lesions calculated for ^{18}F-FDG (A) and ^{68}Ga-FAPI-46 (B) and fold changes of all parameters calculated for ratio of ^{68}Ga-FAPI-46 to ^{18}F-FDG (C). Boxes represent interquartile range, whiskers represent interquartile range of 1.5, and horizontal line within box indicates median. Data outliers are shown separately within graph. *$P < 0.05$. **$P < 0.01$. ns = not significant.

(2 hamartomas, 1 tuberculosis, 1 sarcoidosis, 1 granuloma, 1 calcified lymph node, and 1 lung tissue without evidence of pathology), and 12 patients were diagnosed with LC (11 adenocarcinomas [4 of them with a predominantly lepidic growth pattern] and 1 typical carcinoid). Detailed patientwise information on the clinical status and applied imaging methods is given in Table 1.

CT Size and ^{18}F-FDG and ^{68}Ga-FAPI-46 Uptake of LC and Benign Lesions

LC and benign lesions showed no significant differences in their average CT size or ^{18}F-FDG uptake in terms of SUV_{max}, SUV_{mean}, or corresponding TBR (Figs. 2A and 2B). In contrast, the average ^{68}Ga-FAPI-46 uptake of LC lesions was significantly higher than that of benign lesions (Fig. 2C). Similarly, ratios between ^{68}Ga-FAPI-46 uptake and ^{18}F-FDG uptake were also significantly higher in LC than in benign lesions (Fig. 2D). With respect to benign subentities, moderately higher ^{18}F-FDG and ^{68}Ga-FAPI-46 uptake was seen in sarcoidosis, tuberculosis, and the calcified lymph node than in the other benign lesions (Supplemental Fig. 1; supplemental materials are available at http://jnm.snmjournals.org). Supplemental Table 1 provides a lesion-wise overview of all static PET parameters (SUV_{max}, SUV_{mean}, and corresponding TBR for ^{18}F-FDG and ^{68}Ga-FAPI-46 PET) for all LC and benign lesions analyzed. Figures 3 and 4 show ^{18}F-FDG PET and ^{68}Ga-FAPI-46 images of an example patient with a lepidic LC that had ^{18}F-FDG uptake below the blood pool level and strong ^{68}Ga-FAPI-46 positivity (Fig. 3) and an example patient with a hamartoma that showed only faint uptake of both tracers (Fig. 4).

Dynamic ^{68}Ga-FAPI-46 PET Imaging Characteristics of LC and Benign Lesions

Dynamic ^{68}Ga-FAPI-46 PET imaging was performed on 11 patients with LC and 5 patients with benign lesions. LC and benign

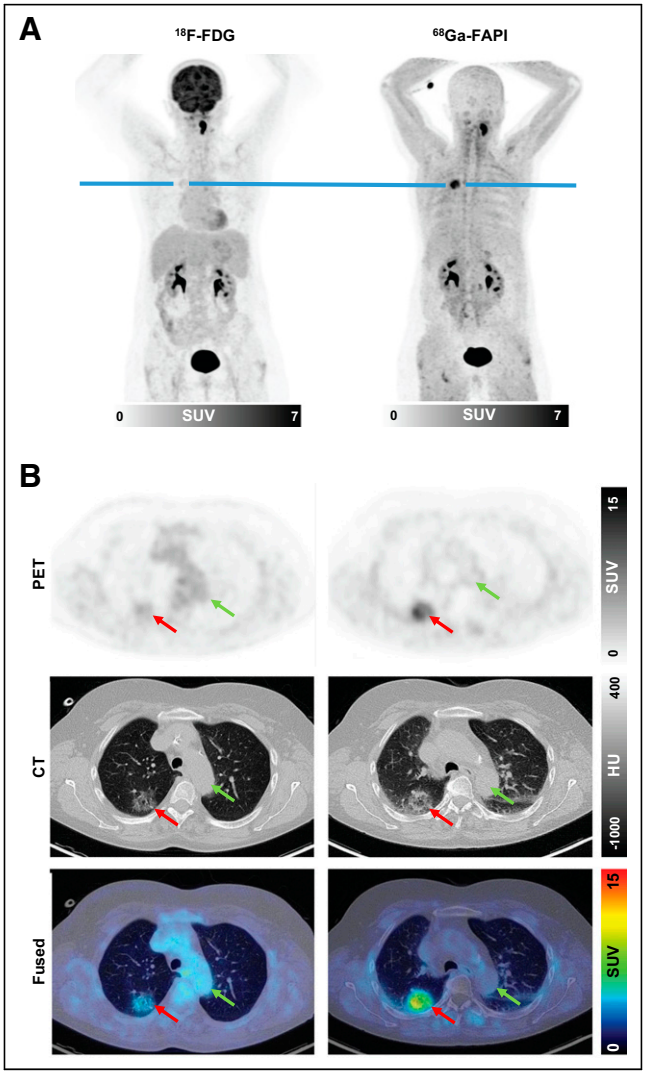

FIGURE 3. Example ^{18}F-FDG and ^{68}Ga-FAPI-46 images of 51-y-old woman with adenocarcinoma with lepidic growth pattern in right upper lobe. (A) Maximum-intensity-projection PET images. (B) Axial images of suggestive lesion (red arrows) with low CT density in right lower lobe. Green arrows show blood pool in aortic arch. Lesion had ^{18}F-FDG uptake below blood pool niveau but was strongly ^{68}Ga-FAPI-46–positive. CT-guided biopsy led to pathologic diagnosis of adenocarcinoma, and patient was treated by stereotactic body radiation therapy because of functional inoperability. HU = Hounsfield units.

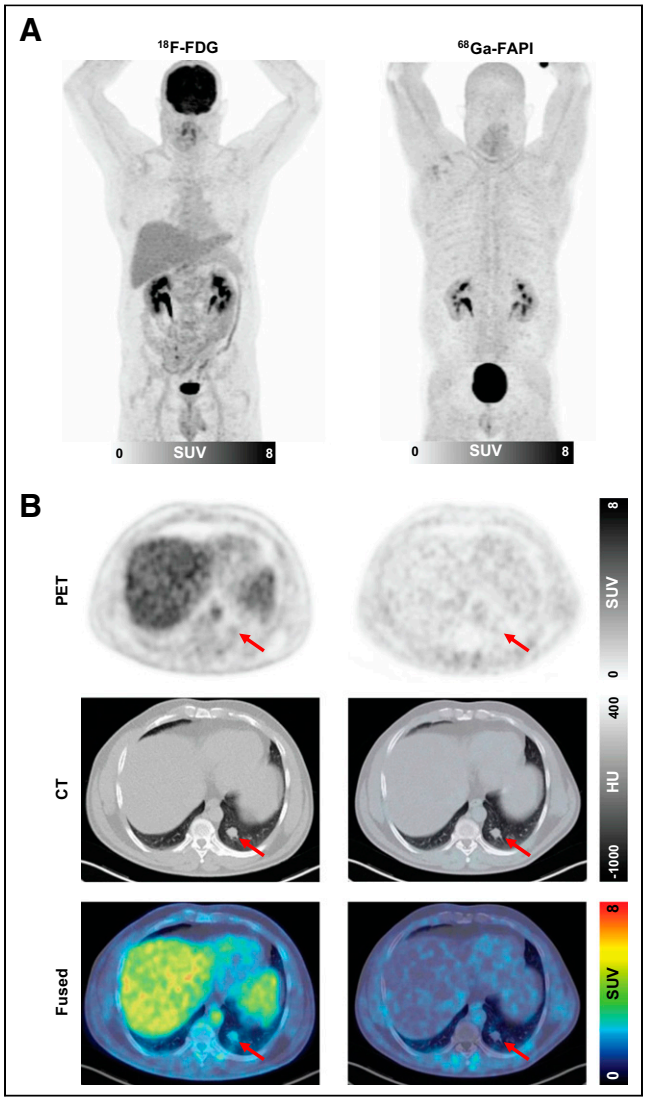

FIGURE 4. Example ^{18}F-FDG and ^{68}Ga-FAPI-46 images of 41-y-old man with hamartoma in left lower lobe. (A) Maximum-intensity-projection PET images. (B) Axial images of suggestive lesion (arrows) in left lower lobe. After wedge resection, hamartoma was diagnosed by pathology. HU = Hounsfield units.

lesions showed marked differences regarding their time–activity curve characteristics. As shown by the averaged time–activity curves in Figure 5A, LC was characterized by a delayed peak at 500–1,000 s after injection followed by a slow, continuous washout phase. In contrast, benign lesions typically showed an early peak within the first 2 min after injection followed by a rapid washout phase resulting in a reduction in activity to approximately 50% at 60 min after injection. Quantitative analysis of time to peak and slope showed a significantly prolonged time to peak and significantly smaller absolute values of slopes for LC than for benign lesions (Fig. 5B). Figure 5C shows 2 cases of LC and sarcoidosis, both of which had intermediate ^{68}Ga-FAPI-46 uptake on static imaging but time–activity curves typical of LC and benign lesions, respectively.

Sensitivity and Specificity of Static and Dynamic ^{68}Ga-FAPI-46 PET Imaging Parameters

Receiver-operating-characteristic curves calculated for all static parameters and for the dynamic parameters time to peak and slope showed high sensitivity and specificity for discriminating LC from benign lesions. The highest areas under the curve were calculated for ^{68}Ga-FAPI-46/^{18}F-FDG SUV_{max} TBR (0.9167), ^{68}Ga-FAPI-46/^{18}F-FDG SUV_{mean} (0.9167), SUV_{mean} TBR (0.8831), and SUV_{max} TBR (0.8571) (Fig. 6). The calculated sensitivity and specificity of ^{68}Ga-FAPI-46/^{18}F-FDG SUV_{max} TBR were 85.71 (95% CI, 48.69–99.27) and 83.33 (95% CI, 55.20–97.04), respectively, for a cutoff of 1.62. The other static and the dynamic ^{68}Ga-FAPI-46 PET parameters showed slightly lower areas under the curve, and the ^{18}F-FDG PET parameters and CT size showed significantly lower areas under the curve (Supplemental Fig. 2).

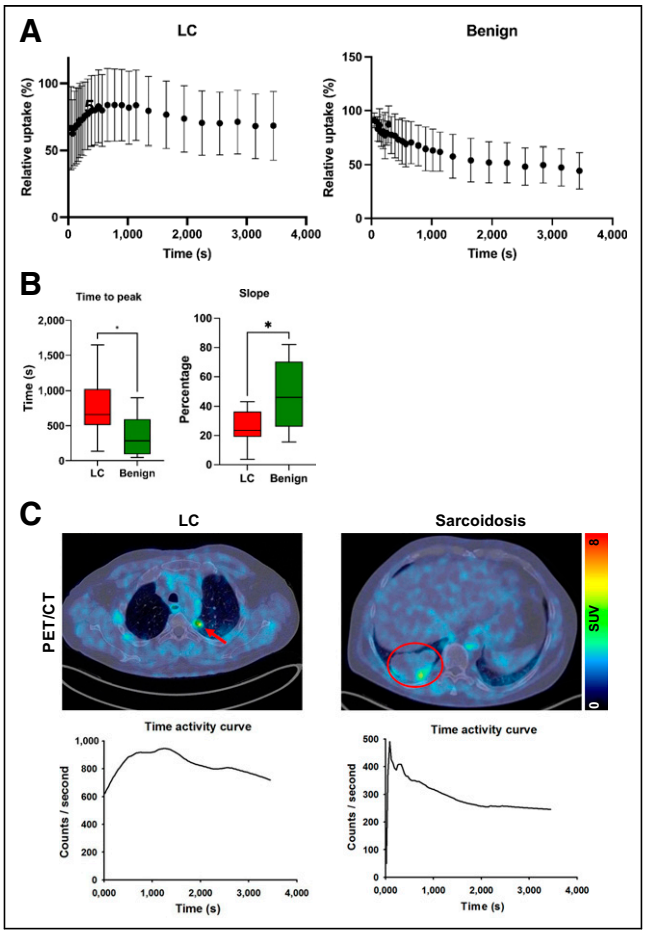

FIGURE 5. Dynamic ^{68}Ga-FAPI-46 PET imaging properties of LC and benign pulmonary lesions. (A) Averaged time–activity curves (relative to peak) of LC and benign pulmonary lesions. (B) Box plot of time to peak and slope of LC and benign pulmonary lesions. Boxes represent interquartile range, whiskers represent interquartile range of 1.5, and horizontal line within box indicates median. (C) Representative cases: 63-y-old man with adenocarcinoma (arrow) of left upper lobe and 62-y-old man with focally ^{68}Ga-FAPI-46–avid sarcoid mass (encircled) in right lower lobe. Images are from static PET, and time–activity curves are from dynamic PET. Although both lesions show intermediate ^{68}Ga-FAPI-46 uptake, time–activity curves clearly differ, with delayed peak of LC and markedly pronounced slope of sarcoidosis. *$P < 0.05$.

DISCUSSION

This retrospective analysis evaluated the ^{68}Ga-FAPI-46 uptake of primary, ^{18}F-FDG–negative LC and benign pulmonary lesions, as well as their kinetic behavior in dynamic ^{68}Ga-FAPI-46 PET imaging. To characterize lepidic LC as a particularly promising ^{18}F-FDG–negative target for ^{68}Ga-FAPI-46 PET, we performed additional FAP immunohistochemistry of 24 tissue sections of lepidic LC and found strong FAP positivity in all specimens. This advance target characterization was of crucial interest for our analysis, as the presence of cancer-associated fibroblasts in lepidic LC has already been described histologically but the FAP expression of this entity had not, to our knowledge, been evaluated before (*23*). The strong FAP expression of lepidic LC is noteworthy because FAP-positive cancer-associated fibroblasts are crucially involved in tumor desmoplasia (*24*,*25*)—a process that is canonically considered a feature of more invasive LC subtypes, but not lepidic LC, as recently proposed by the International Association for the Study of Lung Cancer pathology committee (*26*). However, the results of our immunohistochemical and PET studies seem to indicate that a stromal reaction resulting in FAP positivity of the tumors is present even in early-stage, relatively noninvasive cancers such as lepidic LC.

In our analysis, all cases of LC showed markedly elevated ^{68}Ga-FAPI-46 uptake, increased TBRs, and increased ^{68}Ga-FAPI-46/^{18}F-FDG ratios for all parameters compared with benign pulmonary lesions. One prospective study and large retrospective analyses have demonstrated that ^{68}Ga-FAPI-46 PET in addition to gold standard imaging methods holds high potential for the staging and clinical management of LC (*13*–*15*,*27*). However, these studies were focused on advanced-stage cancers and did not address the value of ^{68}Ga-FAPI-46 PET for the assessment of unclear single pulmonary lesions. In their recent prospective study on 34 patients with advanced, metastatic LC, Wang et al. showed that ^{68}Ga-FAPI PET in addition to ^{18}F-FDG PET/CT detects additional suspected metastases in lymph nodes, brain, bone, and pleura. However, the metabolic tumor volume and SUV_{max} in primary and recurrent primaries were mostly identical for both tracers (*13*). Similarly, Giesel et al. found no significant difference in ^{68}Ga-FAPI and ^{18}F-FDG uptake by primary tumors in 71 patients with various cancers, including 9 patients with LC (*14*). The missing difference in ^{18}F-FDG and ^{68}Ga-FAPI PET signal behavior for LC primaries in these studies might be explained by the inclusion of patients with primary and recurrent stage IV disease only, which is biologically more aggressive and more ^{18}F-FDG–avid than the nonmetastatic ^{18}F-FDG–negative primaries in our analysis. Chen et al. analyzed ^{68}Ga-FAPI– and ^{18}F-FDG–based staging of 54 cancer patients, including 8 with LC, and reported higher SUVs for LC primaries for ^{68}Ga-FAPI than for ^{18}F-FDG. Furthermore, they

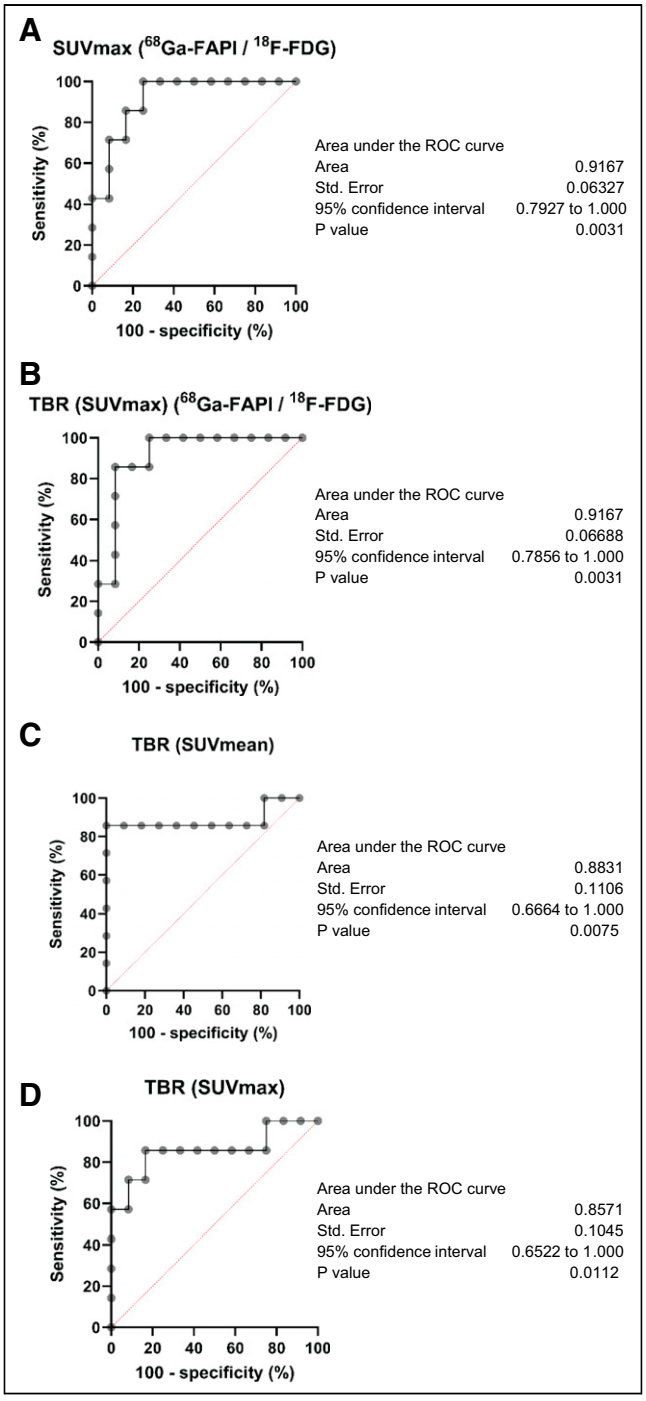

FIGURE 6. Receiver-operating-characteristic (ROC) curves of 4 quantitative PET parameters with highest discriminatory power: ^{68}Ga-FAPI-46/^{18}F-FDG SUV_{max} (A), ^{68}Ga-FAPI-46/^{18}F-FDG TBR SUV_{max} (B), SUV_{mean} TBR (C), and SUV_{max} TBR (D).

included 2 LC cases in which the primary tumor was detectable with ^{68}Ga-FAPI PET but not ^{18}F-FDG PET (*15*). However, because only 2 stage I LC cases were included, there is reduced comparability between their results and ours.

Dynamic imaging analysis revealed differential time–activity curves for LC and benign pulmonary lesions: initially increasing time–activity curves with a decent slope were typical of LC, and steadily decreasing time–activity curve indicated benign pulmonary lesions, as reflected by a significantly increased time to peak and absolute value of the slope for LC. These results are in line with our previously published data on dynamic ^{68}Ga-FAPI-46 PET in LC and fibrosing interstitial lung diseases, intraductal papillary mucinous neoplasms of the pancreas, and pancreatic ductal adenocarcinomas. In that work, we observed similar time–activity curve patterns related to whether tumors were benign or malignant (*20*,*28*). On the basis of our summed experiences, we would generally recommend dynamic ^{68}Ga-FAPI PET acquisition in primary patients with unclear and potentially malignant lesions, such as screening-detected pulmonary lesions.

Relative (^{68}Ga-FAPI-46/^{18}F-FDG) SUV_{max} and TBR showed the highest sensitivity and specificity for the discrimination of LC from benign pulmonary lesions, and the other static and dynamic PET parameters had only slightly lower sensitivity and specificity. CT size, which is in general the most important imaging feature for the risk stratification of pulmonary lesions (*29*,*30*), showed significantly lower sensitivity and specificity for the discrimination of LC from benign lesions, as can be explained by the relatively low number of patients included. The sensitivity and specificity of the ^{68}Ga-FAPI-46 PET–derived parameters calculated for our dataset were similar to those reported for ^{18}F-FDG (*31*,*32*). However, as our dataset included only highly selected ^{18}F-FDG–negative cases, a comparison between the discriminatory power of ^{68}Ga-FAPI-46 PET and ^{18}F-FDG PET for single pulmonary lesions cannot be made.

Our results suggest that supplemental ^{68}Ga-FAPI-46 PET may improve the noninvasive assessment of primary pulmonary lesions compared with ^{18}F-FDG PET and CT alone. Noninvasive assessment of pulmonary lesions is of great clinical relevance because there are several contraindications, such as coagulopathies, reduced cardiopulmonary function, or reduced lung function, that can disfavor surgery or biopsy interventions, especially in elderly patients (*33*). In particular, for lepidic LC, ^{68}Ga-FAPI-46 PET holds great potential to facilitate and accelerate clinical decision making toward biopsy or operative resection, as ^{18}F-FDG PET frequently leads to inconclusive results, and CT-morphologic progression of these slowly growing tumors can be detected only over a relatively long time (*34*). On the other hand, supplemental ^{68}Ga-FAPI-46 PET could be helpful to avoid overtreatment in terms of unnecessary resections, as double-negative (^{18}F-FDG and ^{68}Ga-FAPI-46) lesions appear to have a high probability of being benign. Dynamic imaging can support the assessment of pulmonary lesions in cases without clearly suggestive high or low ^{68}Ga-FAPI-46 uptake. However, the results of our recent analysis should be considered preliminary and hypothesis-generating, and 2 major limitations must be mentioned. First, the number of patients analyzed was relatively small—with the subgroups thus being even smaller, especially with regard to benign subentities. Second, because the patients were highly selected according to ^{18}F-FDG negativity of suggestive pulmonary lesions, our dataset does not allow comparison of the diagnostic accuracy of ^{18}F-FDG and ^{68}Ga-FAPI-46 PET for primary pulmonary lesions in general. Larger, confirmative studies are necessary to gain more evidence on the clinical value of ^{68}Ga-FAPI-46 PET for assessment of primary pulmonary lesions.

CONCLUSION

The intense ^{68}Ga-FAPI-46 uptake of primary, ^{18}F-FDG–negative LC compared with benign pulmonary lesions, as well as their differential kinetic behavior on dynamic ^{68}Ga-FAPI-46 PET imaging, suggests that supplemental ^{68}Ga-FAPI-46 PET may optimize

patient stratification in this clinical scenario. The promising results of this analysis should be confirmed by larger studies.

DISCLOSURE

This work was funded by the Federal Ministry of Education and Research (grant 13N 13341). Uwe Haberkorn has filed a patent application for quinoline-based FAP-targeting agents for imaging and therapy in nuclear medicine and has shares of a consultancy group for iTheranostics. No other potential conflict of interest relevant to this article was reported.

KEY POINTS

QUESTION: Can supplemental ^{68}Ga-FAPI-46 PET help to assess ^{18}F-FDG–negative single pulmonary lesions?

PERTINENT FINDINGS: LC showed markedly elevated ^{68}Ga-FAPI-46 uptake, increased TBRs, and increased ^{68}Ga-FAPI-46/^{18}F-FDG ratios for all parameters compared with benign pulmonary lesions. Dynamic imaging analysis revealed differential time–activity curves for LC and benign pulmonary lesions. Relative (^{68}Ga-FAPI-46/^{18}F-FDG) SUV_{max} and TBR showed the highest sensitivity and specificity for discrimination of LC from benign pulmonary lesions.

IMPLICATIONS FOR PATIENT CARE: Supplemental ^{68}Ga-FAPI-46 PET appears extremely promising in the clinical scenario of ^{18}F-FDG–negative single pulmonary lesions, especially when biopsy or resection is hampered by reduced health status of patients and noninvasive methods are crucial for assessment of malignancy.

REFERENCES

1. Bade BC, Dela Cruz CS. Lung cancer 2020: epidemiology, etiology, and prevention. *Clin Chest Med.* 2020;41:1–24.
2. Ruilong Z, Daohai X, Li G, Xiaohong W, Chunjie W, Lei T. Diagnostic value of ^{18}F-FDG-PET/CT for the evaluation of solitary pulmonary nodules: a systematic review and meta-analysis. *Nucl Med Commun.* 2017;38:67–75.
3. Lococo F, Guerrera F, Rena O, et al. Accuracy of ^{18}F-FDG in detecting stage I lung adenocarcinomas according to IASLC/ATS/ERS classification. *Heart Lung Circ.* 2022;31:726–732.
4. Nakamura H, Saji H, Shinmyo T, et al. Close association of IASLC/ATS/ERS lung adenocarcinoma subtypes with glucose-uptake in positron emission tomography. *Lung Cancer.* 2015;87:28–33.
5. Kratochwil C, Flechsig P, Lindner T, et al. ^{68}Ga-FAPI PET/CT: tracer uptake in 28 different kinds of cancer. *J Nucl Med.* 2019;60:801–805.
6. Mori Y, Dendl K, Cardinale J, Kratochwil C, Giesel FL, Haberkorn U. FAPI PET: fibroblast activation protein inhibitor use in oncologic and nononcologic disease. *Radiology.* 2023;306:e220749.
7. Lindner T, Loktev A, Altmann A, et al. Development of quinoline-based theranostic ligands for the targeting of fibroblast activation protein. *J Nucl Med.* 2018;59:1415–1422.
8. Loktev A, Lindner T, Burger EM, et al. Development of fibroblast activation protein-targeted radiotracers with improved tumor retention. *J Nucl Med.* 2019;60:1421–1429.
9. Loktev A, Lindner T, Mier W, et al. A tumor-imaging method targeting cancer-associated fibroblasts. *J Nucl Med.* 2018;59:1423–1429.
10. Röhrich M, Syed M, Liew DP, et al. ^{68}Ga-FAPI-PET/CT improves diagnostic staging and radiotherapy planning of adenoid cystic carcinomas: imaging analysis and histological validation. *Radiother Oncol.* 2021;160:192–201.
11. Röhrich M, Naumann P, Giesel FL, et al. Impact of ^{68}Ga-FAPI PET/CT imaging on the therapeutic management of primary and recurrent pancreatic ductal adenocarcinomas. *J Nucl Med.* 2021;62:779–786.
12. Giesel FL, Adeberg S, Syed M, et al. FAPI-74 PET/CT using either ^{18}F-AlF or Cold-Kit ^{68}Ga labeling: biodistribution, radiation dosimetry, and tumor delineation in lung cancer patients. *J Nucl Med.* 2021;62:201–207.
13. Wang L, Tang G, Hu K, et al. Comparison of ^{68}Ga-FAPI and ^{18}F-FDG PET/CT in the evaluation of advanced lung cancer. *Radiology.* 2022;303:191–199.
14. Giesel FL, Kratochwil C, Schlittenhardt J, et al. Head-to-head intra-individual comparison of biodistribution and tumor uptake of ^{68}Ga-FAPI and ^{18}F-FDG PET/CT in cancer patients. *Eur J Nucl Med Mol Imaging.* 2021;48:4377–4385.
15. Chen H, Pang Y, Wu J, et al. Comparison of [^{68}Ga]Ga-DOTA-FAPI-04 and [^{18}F] FDG PET/CT for the diagnosis of primary and metastatic lesions in patients with various types of cancer. *Eur J Nucl Med Mol Imaging.* 2020;47:1820–1832.
16. Koerber SA, Rohrich M, Walkenbach L, et al. Impact of ^{68}Ga-FAPI PET/CT on staging and oncologic management in a cohort of 226 patients with various cancers. *J Nucl Med.* 2023;64:1712–1720.
17. Zhou X, Wang S, Xu X, et al. Higher accuracy of [^{68}Ga]Ga-DOTA-FAPI-04 PET/CT comparing with 2-[^{18}F]FDG PET/CT in clinical staging of NSCLC. *Eur J Nucl Med Mol Imaging.* 2022;49:2983–2993.
18. Wei Y, Ma L, Li P, et al. FAPI compared with FDG PET/CT for diagnosis of primary and metastatic lung cancer. *Radiology.* 2023;308:e222785.
19. Bueno J, Landeras L, Chung JH. Updated Fleischner Society guidelines for managing incidental pulmonary nodules: common questions and challenging scenarios. *Radiographics.* 2018;38:1337–1350.
20. Röhrich M, Leitz D, Glatting FM, et al. Fibroblast activation protein-specific PET/CT imaging in fibrotic interstitial lung diseases and lung cancer: a translational exploratory study. *J Nucl Med.* 2022;63:127–133.
21. Cheran SK, Nielsen ND, Patz EF Jr. False-negative findings for primary lung tumors on FDG positron emission tomography: staging and prognostic implications. *AJR.* 2004;182:1129–1132.
22. Maurer GD, Brucker DP, Stoffels G, et al. ^{18}F-FET PET imaging in differentiating glioma progression from treatment-related changes: a single-center experience. *J Nucl Med.* 2020;61:505–511.
23. Yotsukura M, Asamura H, Suzuki S, et al. Prognostic impact of cancer-associated active fibroblasts and invasive architectural patterns on early-stage lung adenocarcinoma. *Lung Cancer.* 2020;145:158–166.
24. Zeltz C, Primac I, Erusappan P, Alam J, Noel A, Gullberg D. Cancer-associated fibroblasts in desmoplastic tumors: emerging role of integrins. *Semin Cancer Biol.* 2020;62:166–181.
25. Lo A, Wang LS, Scholler J, et al. Tumor-promoting desmoplasia is disrupted by depleting FAP-expressing stromal cells. *Cancer Res.* 2015;75:2800–2810.
26. Thunnissen E, Beasley MB, Borczuk A, et al. Defining morphologic features of invasion in pulmonary nonmucinous adenocarcinoma with lepidic growth: a proposal by the International Association for the Study of Lung Cancer pathology committee. *J Thorac Oncol.* 2023;18:447–462.
27. Koerber SA, Rohrich M, Walkenbach L, et al. Impact of ^{68}Ga-FAPI PET/CT on staging and oncologic management in a cohort of 226 patients with various cancers. *J Nucl Med.* 2023;64:1712–1720.
28. Lang M, Spektor AM, Hielscher T, et al. Static and dynamic ^{68}Ga-FAPI PET/CT for the detection of malignant transformation of intraductal papillary mucinous neoplasia of the pancreas. *J Nucl Med.* 2023;64:244–251.
29. Chen B, Li Q, Hao Q, et al. Malignancy risk stratification for solitary pulmonary nodule: a clinical practice guideline. *J Evid Based Med.* 2022;15:142–151.
30. Mazzone PJ, Lam L. Evaluating the patient with a pulmonary nodule: a review. *JAMA.* 2022;327:264–273.
31. Groheux D, Quere G, Blanc E, et al. FDG PET-CT for solitary pulmonary nodule and lung cancer: literature review. *Diagn Interv Imaging.* 2016;97:1003–1017.
32. Cronin P, Dwamena BA, Kelly AM, Carlos RC. Solitary pulmonary nodules: meta-analytic comparison of cross-sectional imaging modalities for diagnosis of malignancy. *Radiology.* 2008;246:772–782.
33. Young M, Sankari A. Percutaneous lung lesion biopsy. StatPearls website. https://www.statpearls.com/point-of-care/30515. Updated February 14, 2024. Accessed March 20, 2024.
34. Hong JH, Park S, Kim H, et al. Volume and mass doubling time of lung adenocarcinoma according to WHO histologic classification. *Korean J Radiol.* 2021;22:464–475.